Inorganic Chemistry

pubs.acs.org/IC

Communication

High Adsorption Capacity and Selectivity of SO_2 over CO_2 in a Metal–Organic Framework

Ya Ling Fan, Hui Ping Zhang, Meng Jia Yin, Rajamani Krishna, Xue Feng Feng,* Li Wang, Ming Biao Luo, and Feng Luo*

Cite This: *Inorg. Chem.* 2021, 60, 4–8

Read Online

ACCESS | Metrics & More | Article Recommendations | Supporting Information

ABSTRACT: Herein, we report a new metal–organic framework (MOF), namely, **ECUT-77**, which is built on rod-shaped secondary building units, showing a high Brunauer–Emmett–Teller surface area of 760.3 cm^2/g, a pore volume of 0.4 cm^3/g, and an aperture of about 1 nm. This MOF enables both high SO_2 adsorption capacity up to 8.0 mmol/g at 0.92 bar and room temperature and a high SO_2/CO_2 selectivity of 44, resulting in excellent SO_2 separation upon a **ECUT-77** column from a SO_2/CO_2 mixture containing 2000 ppm of SO_2.

Recently, metal–organic frameworks (MOFs) were extensively explored.[1−5] This unique porous platform was built on metal ions and organic ligands through coordination bonds, thus showing a myriad of structures and functions. Outstanding host–guest behavior directed by special organic ligands with anchored functionalized units or by metal ions with potential coordination ability impressively enables MOFs with outstanding performance in catalysis and separation.[6−10]

In contrast to traditional distillation techniques, the current major solution in the separation industry, which is often viewed as very extensive, a porous adsorbent-based separation pathway is more desirable because of its low cost and energy. In this regard, MOFs as separation adsorbents were proposed and are now receiving increasing attention.[11,12] Even for some challenging tasks such as C_2H_2/CO_2, C_2H_2/C_2H_4, C_2H_4/C_2H_6, Xe/Kr, and H/D separation, MOFs are also effective.[13−16] However, only very recently was removal of trace SO_2 in flue gas or other SO_2-containing gases upon MOFs explored.[17] This is mainly because most of MOFs cannot survive from SO_2 because of its strong acidity and corrosion.

Removing SO_2 resulting from the utilization of low-grade fossil fuels, such as industrial desulfurization, has emerged as a serious environmental issue.[18] The current state-of-art of desulfurization is based on limestone or organic solvents as the absorbents. However, this can just give a removal of 90–95% SO_2; thus, trace SO_2 is still present in these SO_2-containing products.[19] Thereby, a new solution is urgently needed to eliminate trace SO_2.

Generally, flue gas is mainly composed of N_2 and CO_2, as well as a parts per million level of SO_2. From the viewpoint of SO_2 separation, the major difficulty in desulfurization of flue gas is the strong acidic nature of SO_2 and CO_2 molecules and an extremely lower SO_2 concentration (relative to CO_2), which needs both high SO_2 adsorption capacity and high SO_2 selectivity over CO_2. The first investigation of using MOFs for SO_2 adsorption was executed by Yaghi et al. in 2008.[20] Several benchmark MOFs such as MOF-5, IRMOF-3, MOF-74, MOF-177, MOF-199, and IRMOF-62 were explored. Also MOF-74 was suggested to show good SO_2 adsorption, relative to the commonly used activated carbon. However, because of the sensitivity toward of water molecules for MOF-74, the SO_2 adsorption performance decreases sharply under humidity conditions. FMOF-2 presents a typical flexible framework during SO_2 adsorption, leading to 2.19 mmol/g uptake at 1 bar and 298 K.[21] The simplest framework of two Prussian Blue analogues displayed 2.65 and 2.03 mmol/g SO_2 uptake at 1 bar and 298 K.[22] Although MOFs can be used to adsorb SO_2, until now, only a few MOFs have shown high SO_2 adsorption capacity at 1 bar and 298 K, such as $Ni(bdc)(ted)_{0.5}$ (9.97 mmol/g),[23] MFM-300(In) (8.28 mmol/g),[24] MFM-600 (5.0 mmol/g),[25] MFM-601(12.3 mmol/g),[25] SIFSIX-1-Cu (11.0 mmol/g),[26] SIFSIX-2-Cu-i (6.9 mmol/g),[26] and MFM-170 (17.5 mmol/g).[27] On the other hand, high SO_2 adsorption selectivity is also a dominating factor to determine SO_2/CO_2 separation, especially at diluted conditions. For example, MFM-170 shows a record SO_2 adsorption capacity but just a SO_2/CO_2 selectivity of 28.[27] Accordingly, constructing MOFs with both high SO_2 adsorption capacity and high SO_2/CO_2 selectivity is still a challenging task.

In this work, we show a new MOF, built on rod-shaped secondary building units, showing a high Brunauer–Emmett–Teller (BET) surface area and a pore volume with an aperture of about 1 nm. SO_2 and CO_2 adsorption tests give both high SO_2 uptake and selectivity, suggesting its superior application in SO_2/CO_2 separation. This was further confirmed by breakthrough experiments for a SO_2/CO_2 mixture containing 2000 ppm of SO_2.

Received: September 29, 2020
Published: December 17, 2020

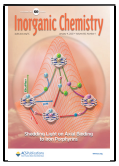

https://dx.doi.org/10.1021/acs.inorgchem.0c02893
Inorg. Chem. 2021, 60, 4–8

The crystals of $Co_2(L)_2(\mu_2\text{-}C_2H_5O)_2$ [**ECUT-77**; HL = 4-(4*H*-1,2,4-triazol-4-yl)benzoic acid; Figure S1] were synthesized by the self-assembly of $Co(NO_3)_2$ and HL in a *N*,*N*-dimethylformamide/C_2H_5OH solution at 115 °C. The yield is up to 80% based on Co. The structure was determined by single-crystal X-ray diffraction, giving a rhombohedral crystal system with the *R*3*c* space group. In **ECUT-77**, there are three crystallographically independent Co^{II} ions. All of the Co sites show a common octahedral geometry (Figure 1a), finished by

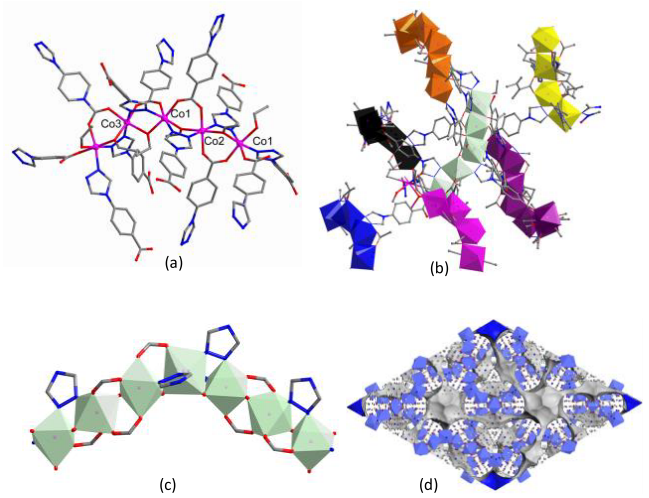

Figure 1. View of the structure of **ECUT-77**. (a) Vertex-sharing octahedral rod composed of Co^{II} ions, μ_2-$C_2H_5O^-$ molecules, and triazole and carboxylate groups. (b and c) Six-connecting rod-shaped secondary building units (each color presents a vertex-sharing octahedral rod). (d) 3D framework with a solvent-accessible void space (white section).

two L^- O atoms, two L^- N atoms, and two μ_2-$C_2H_5O^-$ molecules. There are two crystallographically independent L^- ligands, one being normal and one being disordered, in the triazole and carboxylate sections. In the literature, this kind of disorder was often encountered for such a type of ligand. The C_2H_5OH molecule is deprotonated with a bridging coordination mode.

The secondary building unit in **ECUT-77** is a rod of vertex-sharing octahedra. As shown in Figure 1a, these Co^{II} ions are bridged by μ_2-$C_2H_5O^-$ molecules and triazole and carboxylate groups, generating a 1D chain, where each Co pair, such as Co1Co3 and Co1Co2, is bridged by three connectors composed of a μ_2-$C_2H_5O^-$ molecule and triazole and carboxylate groups. Each vertex-sharing octahedral rod connects to six identical rods via L^- ligands (Figure 1b,c), constructing the overall rod-packing framework (Figure 1d). The solvent-accessible volume estimated by the *PLATON* program[28] is 48.2% of the cell volume (Figure 1d), occupied by disordered solvent molecules.

The thermal stability of **ECUT-77** was initially investigated by thermogravimetric analysis. As shown in Figure S2, because of the continuous weight loss of samples at 30−400 °C, we could not give an exact estimation of its thermal stability, where the loss at 30−200 °C is ascribed to solvent molecules, and after 200 °C the loss could be the removal of coordinated μ_2-$C_2H_5O^-$ molecules and then decomposition of the framework. Interestingly, in the CH_3OH-exchanged samples, a clear platform after 130 °C was observed, and before this temperature, solvent molecules were lost. In this regard, 130 °C was used to activate crystal samples. The powder X-ray diffraction (PXRD) patterns of degassed samples match the data simulated from single-crystal diffraction, confirming the thermal stability of **ECUT-77** (Figure S3). The permanent porosity of degassed samples was obtained by N_2 adsorption at 77 K (Figure 2a), giving a type I microporous feature with a BET surface area of 760.3 cm^2/g and a pore volume of 0.4 cm^3/g. A narrow pore distribution at 1 nm was observed.

The SO_2 adsorption at 298 K is shown in Figures 2b and S4. At 1 bar and 298 K, **ECUT-77** enables high SO_2 uptake up to 8.0 mmol/g, far exceeding the commercial activated carbon (3.3 mmol/g),[26] and is comparable with most reported benchmark MOFs (Table S1),[11] such as $Ni(bdc)(ted)_{0.5}$ (9.97 mmol/g),[23] MFM-300(In) (8.28 mmol/g),[24] MFM-600 (5.0 mmol/g),[25] and SIFSIX-2-Cu-i (6.9 mmol/g).[26] Even at a very low pressure of 0.01 bar, SO_2 uptake is also as high as 2.45 mmol/g, comparable with that of Zn-MOF-74 (3.03 mmol/g),[11,20] one of the top-performing MOFs for such use, suggesting its great potential in flue-gas desulfurization (FGD) applications. Along with the pressure increasing to 0.1 bar, the SO_2 uptake amount is increased more rapidly up to 5.6 mmol/g, higher than that of $Ni(bdc)(ted)_{0.5}$ (3.5 mmol/g)[23] at similar conditions and comparable with those of SIFSIX-2-Cu-i (6.01 mmol/g)[26] and MFM-170 (6.2 mmol/g).[27] By contrast, **ECUT-77** just enables relatively low uptake of CO_2, giving 3.54 mmol/g at 298 K and 1 bar, 0.08 mmol/g at 0.01 bar, and 0.48 mmol/g at 0.1 bar. The corresponding ratio at the same pressure is 2.2, 11.7, and 30.6 for 1, 0.1, and 0.01 bar, implying that **ECUT-77** shows higher SO_2 selectivity at diluted conditions, consequently leading to its superior application in FGD applications. Upon a comparison of the adsorption isotherms of SO_2 with those of CO_2, the adsorption of SO_2 at low pressure is more steep than that of CO_2, indicative of a stronger affinity toward SO_2 than CO_2 from the MOF and, consequently, selective adsorption of SO_2 over CO_2. Moreover, clearly, hysteresis of the desorption of SO_2 was observed, suggesting its stronger affinity from the MOF skeleton, whereas the desorption of CO_2 is reversible, suggesting a physisorption process. To disclose the affinity of the MOF with both SO_2 and CO_2 molecules, the isosteric heats of adsorption (Q_{st}) based on the adsorption data at 298 and 273 K (Figure S5) were calculated, giving 33.3 kJ/mol for SO_2 and 26.6 kJ/mol for CO_2 at the onset of adsorption (Figure 2c), suggesting a higher affinity of the MOF toward SO_2 than CO_2. As seen from Q_{st}, the values of both SO_2 and CO_2 suggest a major physisorption process. The SO_2 selectivity, most likely, is due to the size effect because SO_2 (2.8 Å) has a smaller molecule size than CO_2 (3.3 Å). We further carefully checked the entrance of the pore of **ECUT-77**, which shows a very narrow size of less than 3.0 Å, thus leading to the selective adsorption of SO_2 over CO_2.

The selective adsorption of SO_2 over CO_2 was determined by using ideal adsorbed solution theory calculations for a 1:99 (v/v) SO_2/CO_2 mixture, resulting in ultrahigh selectivity (S = 44−36) at 0.01−1 bar (Figure 2d). The value is bigger than the benchmark MOF of MFM-170 (S = 28).[27] The SO_2 separation ability was initially estimated by the simulated breakthrough. Figure 2e displays the complete separation of SO_2 from a 1:99 (v/v) SO_2/CO_2 mixture with a long separation time ($\Delta\tau$ = 3000). The real SO_2 separation upon the **ECUT-77** bed was next carried out for a SO_2/CO_2 mixture with 2000 ppm of SO_2. As illustrated in Figure 2f, CO_2 emerges from the bed quickly, within 10 min/g, whereas a

https://dx.doi.org/10.1021/acs.inorgchem.0c02893
Inorg. Chem. 2021, 60, 4−8

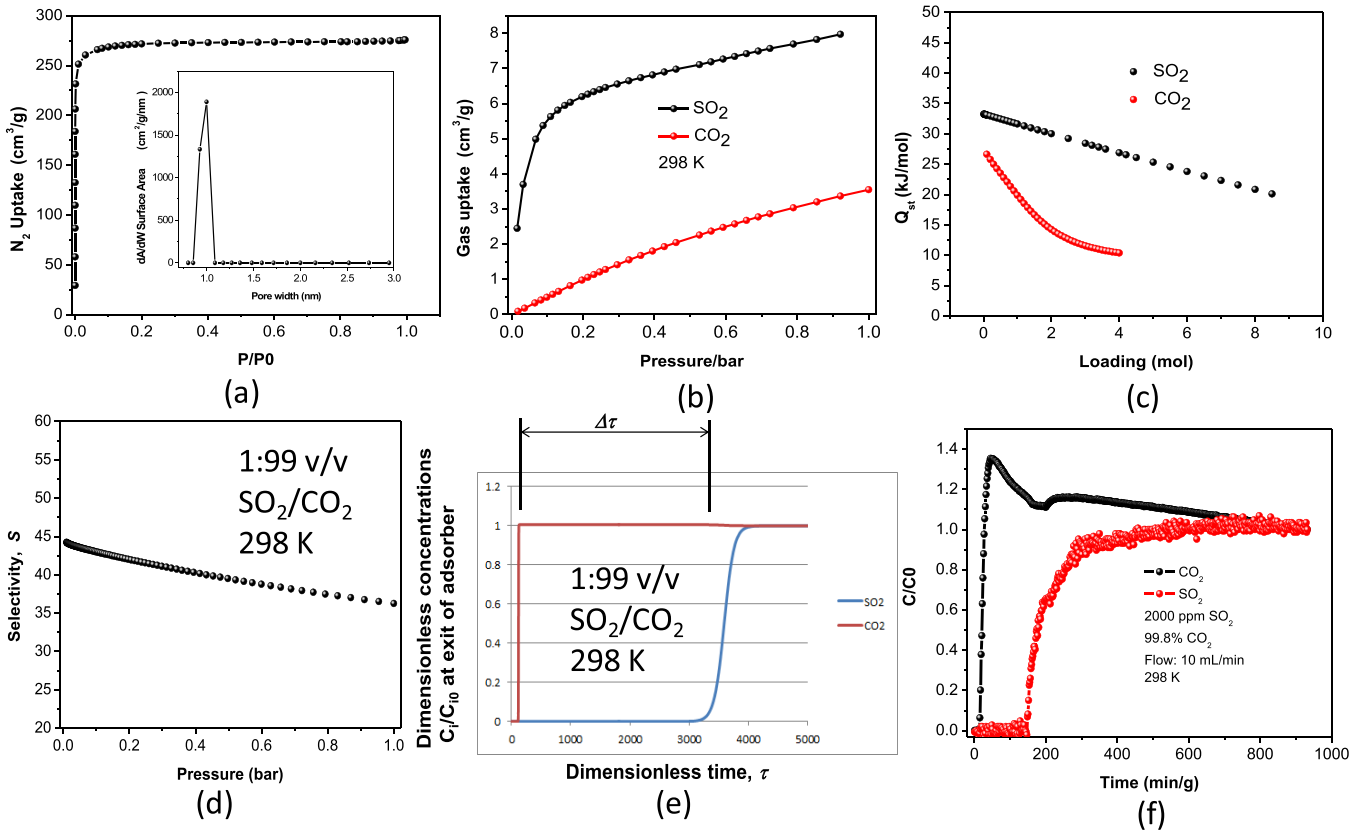

Figure 2. (a) N_2 adsorption isotherms at 77 K. Inset: Pore distribution. (b) SO_2 and CO_2 adsorption isotherms at 298 K. (c) Q_{st} value based on the adsorption data at 298 and 273 K. (d) SO_2/CO_2 selectivity based on a 1:99 (v/v) SO_2/CO_2 mixture at 298 K. (e) Simulated breakthrough for a 1:99 (v/v) SO_2/CO_2 mixture at 298 K. (f) Experimental breakthrough test upon **ECUT-77** (1.6 g) with a flow of 10 mL/min for a SO_2/CO_2 mixture containing 2000 ppm of SO_2.

long retention time was observed for SO_2 as long as 145 min/g, confirming its real SO_2 separation ability for a simulated flue gas. The recycle use was further confirmed (Figure S6). The stability of **ECUT-77** after breakthrough was also confirmed by the PXRD test and the photograph of the samples (Figures S3 and S7). This high chemical stability is mainly due to the rod-shaped secondary building units.

In conclusion, we show in this work a rare case of porous MOF with both high SO_2 adsorption capacity and high SO_2 selectivity over CO_2. These merits including the adsorption capacity and selectivity are comparable with most reported top-performing MOFs for this issue. The practical application of this material for FGD processes was also obtained through breakthrough experiments upon the **ECUT-77** bed.

■ ASSOCIATED CONTENT

Supporting Information

The Supporting Information is available free of charge at https://pubs.acs.org/doi/10.1021/acs.inorgchem.0c02893.

Detailed syntheses and additional figures (PDF)

Accession Codes

CCDC 2033952 contains the supplementary crystallographic data for this paper. These data can be obtained free of charge via www.ccdc.cam.ac.uk/data_request/cif, or by emailing data_request@ccdc.cam.ac.uk, or by contacting The Cambridge Crystallographic Data Centre, 12 Union Road, Cambridge CB2 1EZ, UK; fax: +44 1223 336033.

■ AUTHOR INFORMATION

Corresponding Authors

Xue Feng Feng − *School of Biology, Chemistry and Material Science, East China University of Technology, Nanchang, Jiangxi 344000, China*; Email: 29553800@qq.com

Feng Luo − *School of Biology, Chemistry and Material Science, East China University of Technology, Nanchang, Jiangxi 344000, China*; orcid.org/0000-0001-6380-2754; Email: ecitluofeng@163.com

Authors

Ya Ling Fan − *School of Biology, Chemistry and Material Science, East China University of Technology, Nanchang, Jiangxi 344000, China*

Hui Ping Zhang − *School of Biology, Chemistry and Material Science, East China University of Technology, Nanchang, Jiangxi 344000, China*

Meng Jia Yin − *School of Biology, Chemistry and Material Science, East China University of Technology, Nanchang, Jiangxi 344000, China*

Rajamani Krishna − *Van't Hoff Institute for Molecular Sciences, University of Amsterdam, Amsterdam 1098 XH, The Netherlands*; orcid.org/0000-0002-4784-8530

Li Wang − *School of Biology, Chemistry and Material Science, East China University of Technology, Nanchang, Jiangxi 344000, China*

Ming Biao Luo − *School of Biology, Chemistry and Material Science, East China University of Technology, Nanchang, Jiangxi 344000, China*

https://dx.doi.org/10.1021/acs.inorgchem.0c02893
Inorg. Chem. 2021, 60, 4−8

Complete contact information is available at:
https://pubs.acs.org/10.1021/acs.inorgchem.0c02893

Author Contributions

The manuscript was written through contributions of all authors.

Notes

The authors declare no competing financial interest.

■ ACKNOWLEDGMENTS

We thank the National Science Foundations of China (Grants 21966002, 21871047, and 21761001), the Natural Science Foundation of Jiangxi Province of China (Grant 20181ACB20003), and the Training Program for Academic and Technical Leaders of Major Disciplines in Jiangxi Province (Grant 20194BCJ22010).

■ REFERENCES

(1) (a) Furukawa, H.; Cordova, K. E.; O'Keeffe, M.; Yaghi, O. M. The chemistry and applications of metal-organic frameworks. *Science* **2013**, *341*, 1230444−1230456. (b) Yaghi, O. M.; Kalmutzki, M. J.; Diercks, C. S. *Introduction to reticular chemistry: metal-organic frameworks and covalent organic frameworks*; Wiley-VCH: Weinheim, Germany, 2019.

(2) Li, J.-R.; Kuppler, R. J.; Zhou, H.-C. Selective gas adsorption and separation in metal-organic frameworks. *Chem. Soc. Rev.* **2009**, *38*, 1477−1504.

(3) Cadiau, A.; Adil, K.; Bhatt, P. M.; Belmabkhout, Y.; Eddaoudi, M. A metal-organic framework-based splitter for separating propylene from propane. *Science* **2016**, *353*, 137−140.

(4) Cohen, S. M. Postsynthetic methods for the functionalization of metal-organic frameworks. *Chem. Rev.* **2012**, *112*, 970−1000.

(5) Zhu, L.; Liu, X. Q.; Jiang, H. L.; Sun, L. B. Metal-organic frameworks for heterogeneous basic catalysis. *Chem. Rev.* **2017**, *117*, 8129−8176.

(6) Yang, Q. H.; Xu, Q.; Jiang, H. L. Metal-organic frameworks meet metal nanoparticles: synergistic effect for enhanced catalysis. *Chem. Soc. Rev.* **2017**, *46*, 4774−4808.

(7) Li, L. B.; Lin, R. B.; Krishna, R.; Li, H.; Xiang, S. C.; Wu, H.; Li, J. P.; Zhou, W.; Chen, B. L. Ethane/ethylene separation in a metalorganic framework with iron-peroxo sites. *Science* **2018**, *362*, 443−446.

(8) (a) Liao, P. Q.; Zhang, W. X.; Zhang, J. P.; Chen, X. M. Efficient purification of ethene by an ethane-trapping metal-organic framework. *Nat. Commun.* **2015**, *6*, 8697. (b) Ma, H. F.; Liu, Q. Y.; Wang, Y. L.; Yin, S. G. A water-stable anionic metal-organic framework constructed from columnar zinc-adeninate units for highly selective light hydrocarbon separation and efficient separation of organic dyes. *Inorg. Chem.* **2017**, *56*, 2919−2925. (c) Liu, R.; Liu, Q. Y.; Krishna, R.; Wang, W. J.; He, C. T.; Wang, Y. L. Water-stable europium 1,3,6,8-tetrakis (4-carboxylphenyl)pyrene framework for efficient C_2H_2/CO_2 separation. *Inorg. Chem.* **2019**, *58*, 5089−5095.

(9) (a) Luo, F.; Yan, C. S.; Dang, L. L.; Krishna, R.; Zhou, W.; Wu, H.; Dong, X. L.; Han, Y.; Hu, T. L.; O'Keeffe, M.; Wang, L. L.; Luo, M. B.; Lin, R. B.; Chen, B. L. UTSA-74: a MOF-74 isomer with two accessible binding sites per metal center for highly selective gas separation. *J. Am. Chem. Soc.* **2016**, *138*, 5678−5684. (b) Luo, M. B.; Xiong, Y. Y.; Wu, H. Q.; Feng, X. F.; Li, J. Q.; Luo, F. The MOF^+ technique: a significant synergic effect enables high performance chromate removal. *Angew. Chem., Int. Ed.* **2017**, *56*, 16376−16379. (c) Fan, C. B.; Le Gong, L.; Huang, L.; Luo, F.; Krishna, R.; Yi, X. F.; Zheng, A. M.; Zhang, L.; Pu, S. Z.; Feng, X. F.; Luo, M. B.; Guo, G. C. Significant enhancement of C_2H_2/C_2H_4 separation by a photochromic diarylethene unit: a temperature- and light-responsive separation switch. *Angew. Chem., Int. Ed.* **2017**, *56*, 7900−7906. (d) Yin, W. H.; Xiong, Y. Y.; Wu, H. Q.; Tao, Y.; Yang, L. X.; Li, J. Q.; Tong, X. L.; Luo, F. Functionalizing a metal-organic framework by a photoassisted multicomponent postsynthetic modification approach showing highly effective Hg(II) removal. *Inorg. Chem.* **2018**, *57*, 8722−8725. (e) Xu, Z. Z.; Xiong, X. H.; Xiong, J. B.; Krishna, R.; Li, L. B.; Fan, Y. L.; Luo, F.; Chen, B. L. A robust Th-azole framework for highly efficient purification of C_2H_4 from a $C_2H_4/C_2H_2/C_2H_6$ mixture. *Nat. Commun.* **2020**, *11*, 3163.

(10) Wang, Y. L.; Liu, W.; Bai, Z. L.; Zheng, T.; Silver, M. A.; Li, Y. X.; Wang, Y. X.; Wang, X.; Diwu, J.; Chai, Z. F.; Wang, S. A. Employing a unique unsaturated Th^{4+} site in a porous thorium-organic framework for Kr/Xe uptake and separation. *Angew. Chem., Int. Ed.* **2018**, *57*, 5783−5787.

(11) Wang, C.; Zhou, D. D.; Gan, Y. W.; Zhang, X. W.; Ye, Z. M.; Zhang, J. P. A partially fluorinated ligand for two super-hydrophobic porous coordination polymers with classic structures and increased porosities. *Natl. Sci. Rev.* **2020**, DOI: 10.1093/nsr/nwaa094.

(12) Jaramillo, D. E.; Reed, D. A.; Jiang, Z. H.; Oktawiec, J.; et al. Selective nitrogen adsorption via backbonding in a metal-organic framework with exposed vanadium sites. *Nat. Mater.* **2020**, *19*, 517−521.

(13) Li, B.; Wen, H. M.; Zhou, W.; Xu, J. Q.; Chen, B. L. Porous metal-organic frameworks: promising materials for methane storage. *Chem.* **2016**, *1*, 557−580.

(14) Cui, X. L.; Chen, K. J.; Xing, H. B.; Yang, Q. W.; Krishna, R.; Bao, Z. B.; Wu, H.; Zhou, W.; Dong, X. L.; Han, Y.; Li, B.; Ren, Q. L.; Zaworotko, M. J.; Chen, B. L. Pore chemistry and size control in hybrid porous materials for acetylene capture from ethylene. *Science* **2016**, *353*, 141−144.

(15) Shi, Z. L.; Tao, Y.; Wu, J. S.; Zhang, C. Z.; He, H. L.; Long, L. L.; Lee, Y. J.; Li, T.; Zhang, Y. B. Robust metal-triazolate frameworks for CO_2 capture from flue gas. *J. Am. Chem. Soc.* **2020**, *142*, 2750−2754.

(16) Peng, Y. L.; Pham, T.; Li, P. F.; Wang, T.; Chen, Y.; Chen, K. J.; Forrest, K. A.; Space, B.; Cheng, P.; Zaworotko, M. J.; Zhang, Z. J. Robust ultramicroporous metal-organic frameworks with benchmark affinity for acetylene. *Angew. Chem., Int. Ed.* **2018**, *57*, 10971−10975.

(17) (a) Han, X.; Yang, S. H.; Schröder, M. Porous metal-organic frameworks as emerging sorbents for clean air. *Nat. Rev. Chem.* **2019**, *3*, 108−118. (b) Martínez-Ahumada, E.; Díaz-Ramírez, M. L.; Lara-García, H. A.; Williams, D. R.; Martis, V.; Jancik, V.; Lima, E.; Ibarra, I. A. High and reversible SO2 capture by a chemically stable Cr(III)-based MOF. *J. Mater. Chem. A* **2020**, *8*, 11515−11520. (c) Gorla, S.; Díaz-Ramírez, M. L.; Abeynayake, N. S.; Kaphan, D. M.; Williams, D. R.; Martis, V.; Lara-García, H. A.; Donnadieu, B.; Lopez, N.; Ibarra, I. A.; Montiel-Palma, V. Functionalized NU-1000 with an iridium organometallic fragment: SO_2 capture enhancement. *ACS Appl. Mater. Interfaces* **2020**, *12*, 41758−41764. (d) Zárate, J. A.; Sánchez-González, E.; Williams, D. R.; González-Zamora, E.; Martis, V.; Martínez, A.; Balmaseda, J.; Maurin, G.; Ibarra, I. A. High and energy-efficient reversible SO_2 uptake by a robust Sc(III)-based MOF. *J. Mater. Chem. A* **2019**, *7*, 15580−15584. (e) Mukherjee, S.; Sensharma, D.; Chen, K. J.; Zaworotko, M. J. Crystal engineering of porous coordination networks to enable separation of C_2 hydrocarbons. *Chem. Commun.* **2020**, *56*, 10419−10441. (f) Liang, J.; Xing, S. H.; Brandt, P.; Nuhnen, A.; Schlüsener, C.; Sun, Y. Y.; Janiak, C. A chemically stable cucurbit uril-based hydrogen-bonded organic framework for potential SO_2/CO_2 separation. *J. Mater. Chem. A* **2020**, *8*, 19799−19804.

(18) United States Environmental Protection Agency. Sulfur oxides control technology series: flue gas desulfurization magnesium oxide process. *Summary Report No. 4/1981*; EPA, 1981.

(19) Mathieu, Y.; Tzanis, L.; Soulard, M.; Patarin, J.; Vierling, M.; Molière, M. Adsorption of SO_x by oxide materials: a review. *Fuel Process. Technol.* **2013**, *114*, 81−100.

(20) Britt, D.; Tranchemontagne, D.; Yaghi, O. M. Metal-organic frameworks with high capacity and selectivity for harmful gases. *Proc. Natl. Acad. Sci. U. S. A.* **2008**, *105*, 11623−11627.

(21) Fernandez, C. A.; Thallapally, P. K.; Motkuri, R. K.; Nune, S. K.; Sumrak, J. C.; Tian; Liu, J. Gas-induced expansion and contraction

of a fluorinated metal-organic framework. *Cryst. Growth Des.* **2010**, *10*, 1037−1039.
(22) Thallapally, P. K.; Motkuri, R. K.; Fernandez, C. A.; McGrail, B. P.; Behrooz, G. S. Prussian blue analogues for CO_2 and SO_2 capture and separation applications. *Inorg. Chem.* **2010**, *49*, 4909−4915.
(23) Tan, K.; Canepa, P.; Gong, Q. H.; Liu, J.; et al. Mechanism of preferential adsorption of SO_2 into two microporous paddle wheel frameworks $M(bdc)(ted)_{0.5}$. *Chem. Mater.* **2013**, *25*, 4653−4662.
(24) Savage, M.; Cheng, Y. Q.; Easun, Ti. L.; Eyley, J. E.; Argent, S. P.; Warren, M. R.; Lewis, W.; Murray, C.; Tang, C. C.; Frogley, M. D.; Cinque, G.; Sun, J. L.; Rudić, S.; Murden, R. T.; Benham, M. J.; Fitch, A. N.; Blake, A. J.; Ramirez-Cuesta, A. J.; Yang, S. H.; Schröder, M. Selective adsorption of sulfur dioxide in a robust metal-organic framework material. *Adv. Mater.* **2016**, *28*, 8705−8711.
(25) Carter, J. H.; Han, X.; Moreau, F. Y.; da Silva, I.; Nevin, A.; Godfrey, H. G. W.; Tang, C. C.; Yang, S. H.; Schröder, M. Exceptional adsorption and binding of sulfer dioxide in a robust zirconium-based metal-organic framework. *J. Am. Chem. Soc.* **2018**, *140*, 15564−15567.
(26) Cui, X.; Yang, Q. W.; Yang, L. F.; Krishna, R.; Zhang, Z. G.; Bao, Z. B.; Wu, H.; Ren, Q. L.; Zhou, W.; Chen, B. L.; Xing, H. B. Ultrahigh and selective SO_2 uptake in inorganic anion-pillared hybrid porous materials. *Adv. Mater.* **2017**, *29*, 1606929.
(27) Smith, G. L.; Eyley, J. E.; Han, X.; Zhang, X. R.; Li, J. N.; Jacques, N. M.; Godfrey, H. G. W.; Argent, S. P.; McCormick McPherson, L. J.; Teat, S. J.; Cheng, Y. Q.; Frogley, M. D.; Cinque, G.; Day, S. J.; Tang, C. C.; Easun, T. L.; Rudić, S.; Ramirez-Cuesta, A. J.; Yang, S. H.; Schröder, M. Reversible coordinative binding and separation of sulfur dioxide in a robust metal-organic framework with open copper sites. *Nat. Mater.* **2019**, *18*, 1358−1365.
(28) Blatov, V. A.; Shevchenko, A. P. *TOPOS 4.0*; Samara State University: Samara Oblast, Russia, 1999.

https://dx.doi.org/10.1021/acs.inorgchem.0c02893
Inorg. Chem. 2021, 60, 4−8

High Adsorption Capacity and Selectivity of SO_2 over CO_2 in Metal-Organic Framework

Ya Ling Fan,[a] Hui Ping Zhang,[a] Meng Jia Yin,[a] Rajamani Krishna,[b] Xue Feng Feng,*[a] Li Wang,[a] Ming Biao Luo,[a] and Feng Luo[a]*

[a]School of Biology, Chemistry and Material Science, East China University of Technology, Nanchang, Jiangxi 344000, China

[b]Van't Hoff Institute for Molecular Sciences, University of Amsterdam, Science Park 904, 1098 XH Amsterdam, The Netherlands

Experimental Methods

Materials and Physical Measurements. All chemicals are directly purchased from innochem with no further purification. The data of X-ray powder diffraction were collected on a Bruker AXSD8 Discover powder diffractometer at 40 kV/40 mA for Cu Kα (λ = 1.5406 Å) at room temperature in the range of 5-50 °(2θ) with a scan speed of 0.1 °per step. Thermogravimetric analysis (TG) was performed by a TGA Q500 thermal analysis system. All TGA experiments were performed under a N_2 atmosphere from 40-800°C at a rate of 5°C /min. The gas sorption isotherms were collected on ASAP2020 PLUS (anti-corrosion version). Ultrahigh-purity-grade (>99.999%) N_2, CO_2, and SO_2 gases were used in this adsorption measurement. To maintain the experimental temperatures liquid nitrogen (77 K) and temperature-programmed water bath (273 and 298 K) were used respectively.

Synthesis of ECUT-77. 4-(4H- 1,2,4-triazol-4-yl)benzoic acid (0.1 mmol), $Co(NO_3)_2$ (0.1 mmol), were dissolved in a mixture of 2 mL C_2H_5OH and 3 mL DMF. The solution was moved into a 25 mL Teflon-lined stainless steel vessel and heated at 115 °C for 3 days. Then it is cooled down to room temperature. Red crystals were filtered and washed with 10 mL methyl alcohol and 10 mL deionized water.

Degassing ECUT-77. 100 mg MOF crystals were soaked in methanol for 3d and fresh methanol was added every 8 h. After decanting the methanol extract, the sample was dried at room temperature overnight, then further degassed using ASAP2020 PLUS for 24 h at 130°C.

X-ray Crystallography. X-ray diffraction data of **ECUT-77** were collected at room temperature on a Bruker Appex II CCD diffractometer using graphite monochromated MoKα radiation (λ=0.71073 Å). The data reduction included a correction for Lorentz and polarization effects, with an applied multi-scan absorption correction (SADABS). The crystal structure was solved and refined using the SHELXTL program suite. Direct methods yielded all non-hydrogen atoms, which were refined with anisotropic thermal parameters. All hydrogen atom positions were calculated geometrically and were riding on their respective atoms. The SQUEEZE subroutine of the PLATON software suite was used to remove the scattering from the highly disordered guest molecules. CCDC 2033952 contains the supplementary crystallographic data of **ECUT-77**. These data can be obtained free of charge from the Cambridge Crystallographic Data Centre via www.ccdc.cam.ac.uk/data_request/cif.

Isosteric heat of adsorption

The binding energy is reflected in the isosteric heat of adsorption, Q_{st}, is calculated from the Clausius-Clapeyron equation.

$$Q_{st} = -RT^2 \left(\frac{\partial \ln p}{\partial T} \right)_q$$

IAST calculations of adsorption selectivities and uptake capacities

We consider the separation of binary SO_2/CO_2 1:99 v/v mixtures at 298 K. The adsorption selectivity for SO_2/CO_2 separation is defined by

$$S_{ads} = \frac{q_1/q_2}{p_1/p_2}$$

Transient breakthrough simulations

The performance of industrial fixed bed adsorbers is dictated by a combination of adsorption selectivity and uptake capacity. Transient breakthrough simulations were carried out using the methodology described in earlier publications (*Microporous Mesoporous Mater.* **2014**, *185*, 30-50; *Sep. Purif. Technol.* **2018**, *194*, 281-300; *ACS Omega* **2020**, *5*, 16987−17004). The SO_2/CO_2 1:99 v/v mixture was investigated.

For the breakthrough simulations, the following parameter values were used: length of packed bed, $L = 0.3$ m; voidage of packed bed, $\varepsilon = 0.4$; superficial gas velocity at inlet, $u = 0.04$ m/s.

The *y*-axis is the dimensionless concentrations of each component at the exit of the fixed bed, c_i/c_{i0} normalized with respect to the inlet feed concentrations. The *x*-axis is the *dimensionless* time, $\tau = \frac{tu}{L\varepsilon}$, defined by dividing the actual time, *t*, by the characteristic time, $\frac{L\varepsilon}{u}$.

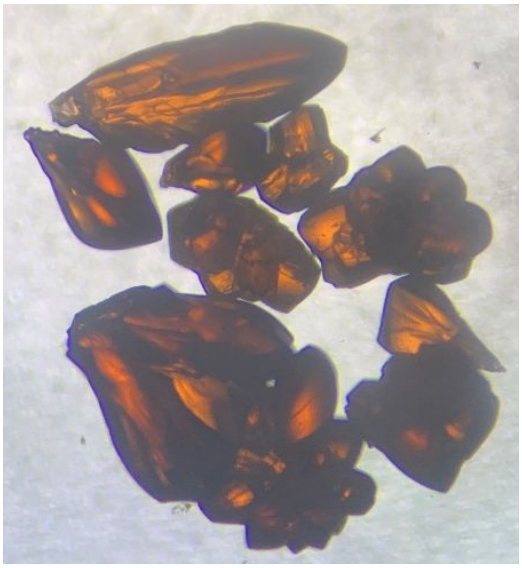

Figure S1. Photograph of **ECUT-77.**

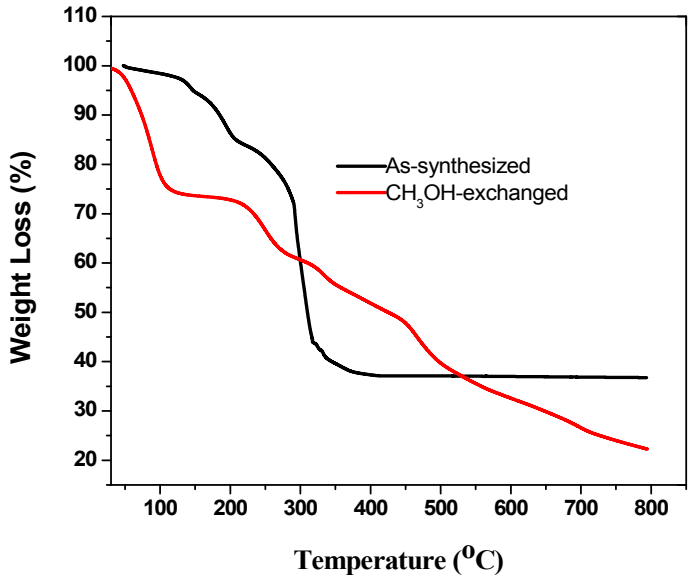

Figure S2. The TG plot of **ECUT-77** and the CH_3OH-exchanged samples.

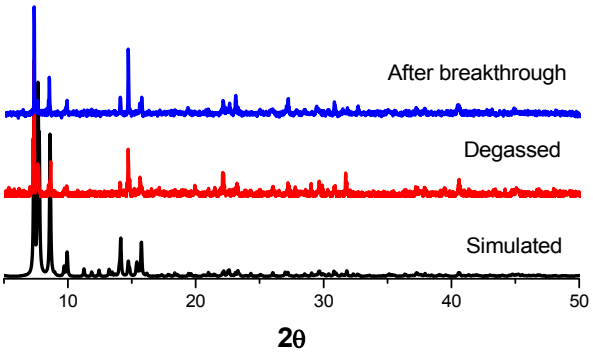

Figure S3. A comparison of PXRD patterns simulated from the single crystal data, and PXRD patterns of degassed samples, and samples after breakthrough.

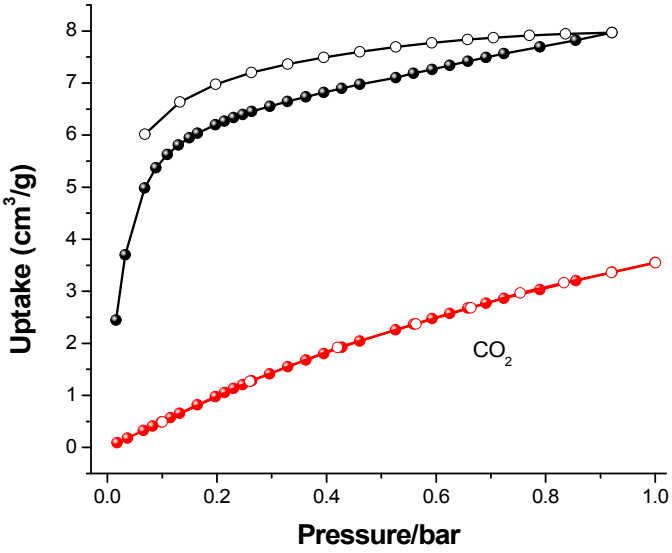

Figure S4. The SO_2 and CO_2 adsorption and desorption isotherms at 298 K. Clearly, hysteresis of desorption was observed SO_2, suggesting its stronger affinity from MOF skeleton, whereas the desorption of CO_2 is reversible, suggesting physisorption process.

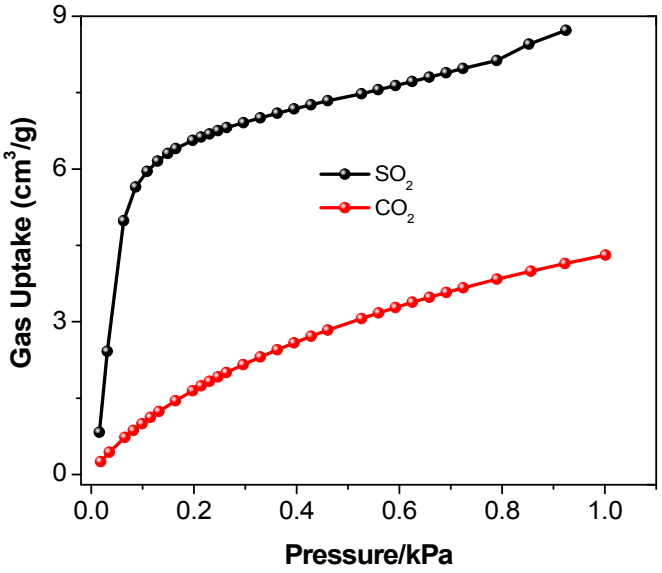

Figure S5. The SO_2 and CO_2 adsorption at 273 K.

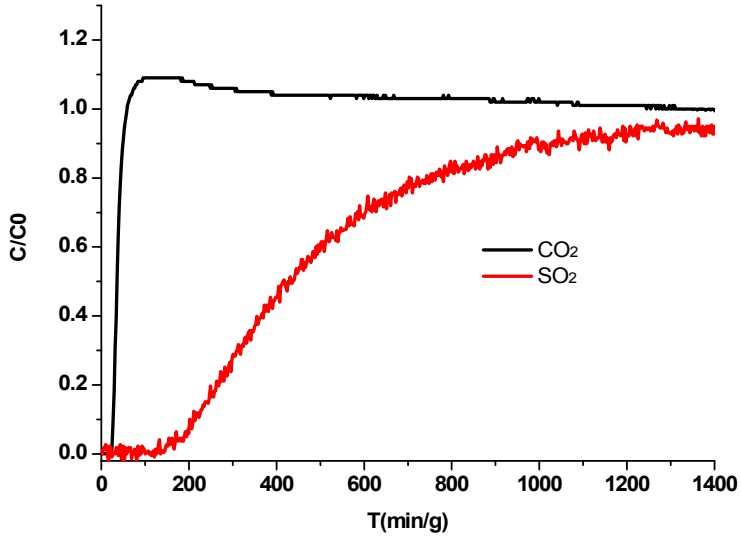

Figure S6. The second breakthrough test upon **ECUT-77** column.

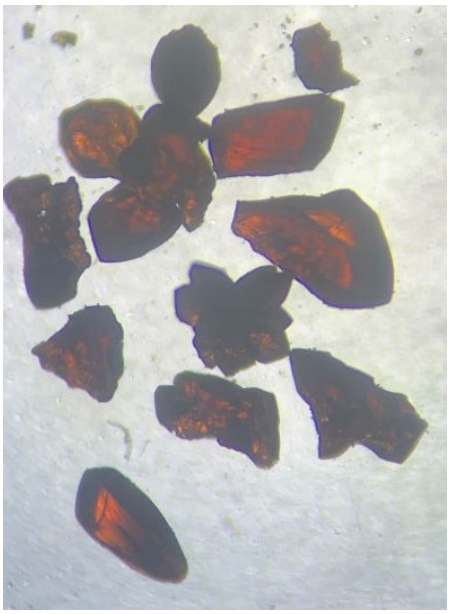

Figure S7. Photograph of the samples after breakthrough test.

Table S1. A comparison of reported MOFs for SO_2 removal.

MOF tpyes	SO_2 adsorption capacity (1 bar, 298 K), mmol/g	SO_2/CO_2 selectivity	References
SIFSIX-2-Cu-i	11.0	87.1	1
$Ni(bdc)(ted)_{0.5}$	9.97	-	2
MFM-300(In)	8.28	50	3
MFM-202a	10.2	-	4
NOTT-300 (Al)	7.1	-	5
MFM-170	17.5	28	6
MOF-5	Less than 0.016	-	7
IRMOF-3	0.094	-	7
MOF-74	3.03	-	7

MOF-199	0.5	-	7
P(TMGA-co-MBA)	4.0	-	8
Activated Carbon	3.3	-	9
ECUT-77	8.0	44	Our work

"-" denotes the data can not be obtaind from corresponding reference.

1.Cui. X. L.; Yang. Q. W.; Yang. L. F.; Krishna. R.; Zhang. Z. G.; Bao. Z. B.; Wu. H.; Ren. Q.; Zhou. W.; Chen. B. L.; Xing. H. B. Ultrahigh and selective SO_2 uptake in inorganic anion-pillared hybrid porous materials. *Advanced Materials*. **2017**. *29*.1606929(1-9).

2. Tan. K.; Canepa. P.; Gong. Q. H.; Liu. J.; Johnson. D. H.; Dyevoich. A.; Thallapally. P. K.; Thonhauser. T.; Li. J.; Chabal. Y. J. Mechanism of preferential adsorption of SO_2 into two microporous paddle wheel frameworks M(bdc)(ted)$_{(0.5)}$. *Chemistry of Materials*. **2013**. *25*. 4653-4662.

3. Savage. M.; Cheng .Y. Q.; Easun. T. L.; Eyley. J. E.; Argent.S. P.; Warren. M. R.; Lewis. W.; Murray. C.; Tang. C. C.; Frogley. M. D.; Cinque G.; Sun. J. L.; Rudic´. S.; Murden R. T.; Benham. M. J.; Fitch. A. N.; Blake. A. J.; Ramirez-Cuesta. A. J.; Yang. S. H.; Schroder. M. Selective Adsorption of Sulfur Dioxide in a Robust Metal–Organic Framework Material. *Advanced Materials*. **2016**. *28*. 8705-8711.

4. Yang. S. H.; Liu. L. F.; Sun. J. L.; Thomas. K. M.; Davies A. J.; George. M. W.; Blake. A. J.; Hill. A. H.; Fitch. A. N.; Tang. C. C. , Chroeder. M. Irreversible network transformation in a dynamic porous host catalyzed by sulfur dioxide. *Journal of the American Chemical Society*. **2013**. *135*. 4954-4957.

5. Yang. S. H.; Sun. J. L.; Ramirez-Cuesta. A. J.; Callear. S. K.; David. W. F.; Anderson. D. P.; Newby. R.; Blake1. A. J.; Parker. J. E.; Tang. C. C.; Schro ¨ der1. M. Selectivity and direct visualization of carbon dioxide and sulfur dioxide in a decorated porous host. *Nature chemistry.* **2012**. *4*.887-894.

6. Smith. G. L.; Eyley. J. E.; Han. X.; Zhang. X. R.; Li. J. N.; Jacques. N. M.; Godfrey. H. G. W.; Argent. S. P.; McPherson. L. J. M.; Teat. S. J.; Cheng Y. Q.; Frogley. M. D.; Cinque. G.; Day S. J.; C. C. Tang.; Easun . T. L.; Rudić. S.; Ramirez-Cuesta . A. J.; Yang. S.H.; Schro ¨ der1. M. Reversible coordinative binding and separation of sulfur dioxide in a robust metal–organic framework with open copper sites. *Nature Materials.* **2019**. *18*. 1358-1365.

7. Britt. D.; Tranchemontagne. D.; Yaghi O. M. Metal-organic frameworks with high capacity and selectivity for harmful gases. *Proceedings of the National Academy of Sciences of the United States of America*. **2008**. *105*. 11623-11627.

8. Wu. L. B.; An. D.; Dong. J.; Zhang. Z. M.; Li. B. G.; Zhu. S. P. Preparation and SO2 Absorption/Desorption Properties of Crosslinked Poly(1,1,3,3-Tetramethylguanidine Acrylate) Porous Particles. *Macromolecular Rapid Communications*. **2006**. *37*.1949-1954.

9. Yi. H. H.; Wang. Z. X.; Liu. H.Y.; Tang X. L.; Ma. D.; Zhao. S. Z.; Zhang. B. W.; Gao. F. Y.; Zuo Y. R. Adsorption of SO_2, NO, and CO_2 on Activated Carbons: Equilibrium and Thermodynamics . *Journal of Chemical & Engineering Data.* **2014**. *59*. 1556-1563.